Green Chemistry

PAPER

View Article Online
View Journal | View Issue

Cite this: *Green Chem.*, 2025, **27**, 15161

Highly energy-efficient hydrogenolysis of high-density polyethylene *via* hydrogen nonthermal plasma reaction engineering

Parsa Pishva, Jinyao Tang, Yanlin Zhu, Jochen Lauterbach and Zhenmeng Peng *

The global surge in synthetic plastic production has resulted in massive waste accumulation and environmental pollution, with most polyolefins ending up in landfills and only a small fraction being downcycled into low-value products. While chemical upcycling offers a sustainable alternative, conventional approaches such as pyrolysis and catalytic hydrogenolysis suffer from slow kinetics, high energy demands, and reliance on costly catalysts. Here, we report the first demonstration of a highly energy-efficient, noncatalytic hydrogenolysis process for high-density polyethylene (HDPE) using dielectric barrier discharge (DBD) nonthermal plasma (NTP) operated under ambient temperature and pressure. Through integrated reactor and reaction engineering, we achieve complete conversion of both pure and real waste HDPE within minutes, producing valuable C_1–C_4 light hydrocarbons and waxes. Mechanistic investigations reveal that optimized plasma–polymer interactions and precisely tuned plasma species energetics and density are critical for maximizing energy efficiency. The system reaches a record output-to-input energy ratio of 8.2 and an electricity cost as low as 2.7 cents per kg of HDPE, far surpassing previously reported NTP-based hydrogenolysis approaches. Notably, waste HDPE yields even higher output energy, confirming the robustness and practical relevance of the process. This work establishes a scalable, low-energy, and catalyst-free platform for sustainable plastic upcycling, offering a transformative and economically viable pathway for converting polyolefin waste into valuable chemical products using ambient, electricity-driven plasma technology.

Received 12th August 2025,
Accepted 31st October 2025

DOI: 10.1039/d5gc04228c

rsc.li/greenchem

Green foundation

1. Our work advances green chemistry by enabling energy-efficient upcycling of waste HDPE into valuable hydrocarbons using nonthermal plasma under mild conditions. This scalable process avoids heat, pressure, and toxic solvents, achieving record energy efficiency and minimal environmental impact while supporting a circular plastics economy.
2. We achieved complete conversion of waste HDPE to valuable C_1–C_4 hydrocarbons and wax under ambient conditions without catalysts or solvents, reaching a record output-to-input energy ratio of 8.2 and an electricity cost as low as 2.7 ¢ per kg.
3. Our work could be made greener by integrating renewable electricity for plasma and hydrogen generation and optimizing product selectivity toward higher-value chemicals. Further research on reactor scaling, life-cycle analysis, and processing mixed plastic streams will enhance sustainability and broaden impact.

Introduction

Over the past century, the global production of synthetic plastics has surged dramatically, and plastic waste is projected to exceed 25 billion tons by 2050, highlighting the urgent need for sustainable upcycling solutions.[1–3] Driven by their versatility, durability, and cost-effectiveness, plastics have become indispensable across many aspects in modern life, enhancing food safety, healthcare, textiles, consumer electronics, and transportation efficiency.[1,4] However, their widespread use, particularly single-use plastics that account for about 60% of total production, has led to an escalating environmental crisis, with over 90% of plastics in the U.S. not being recycled.[5,6] The packaging industry alone contributes nearly half of all plastic waste, with polyethylene (PE) as the dominant component.[4] Alarmingly, most plastic wastes end up in landfills or the natural environment, causing significant pollution to ecosystems. According to a 2017 report, of the 6300 million tons of

Department of Chemical Engineering, University of South Carolina, Columbia, SC 29208, USA. E-mail: zmpeng@sc.edu

plastic waste produced, 79% have been landfilled, 12% incinerated, and only 9% recycled.[7,8] Conventional recycling primarily relies on mechanical methods, such as shredding, heating, and remolding plastics,[9–11] but these approaches often degrade polymer properties, yielding low-quality materials unsuitable for high-performance applications.[11–13] By contrast, chemical upcycling, where waste plastics are converted into higher-value chemicals and fuels, offers a more viable pathway for recovering valuable carbon resources.[14–16] Despite this potential, upcycling polyolefins such as high-density polyethylene (HDPE) remains challenging because of the stability of their strong C–C covalent bonds. These bonds often require harsh conditions, such as high temperatures, elevated pressures, and the use of catalysts, to be effectively broken.[17,18] Thermochemical methods such as pyrolysis, gasification, and catalytic cracking are widely investigated (Fig. 1a and b), but they suffer from slow reaction kinetics, significant heat losses, and reliance on costly catalysts, limiting their economic feasibility.[11,19–22]

Thermocatalytic hydrogenolysis has recently emerged as a promising approach to depolymerize HDPE under milder conditions.[23–25] Unlike pyrolysis, which typically requires extreme temperatures, hydrogenolysis enables exothermic cleavage of polymer chains at comparatively lower temperatures.[14] However, conventional hydrogenolysis methods, whether solvent-based or solvent-free (Fig. 1c), still necessitate elevated temperatures, high hydrogen pressures, and expensive metal catalysts such as platinum (Pt) and ruthenium (Ru).[14,23,26] Although solvent-based hydrogenolysis can operate at lower temperatures (<300 °C), it faces significant challenges including inefficient hydrogen mass transfer, complex product separation, solvent degradation, and environmental concerns from solvent disposal.[27,28] Solvent-free hydrogenolysis eliminates solvent-related issues but demands higher reaction temperatures, leading to greater energy consumption and higher operational costs. Moreover, real-world plastic waste often contains impurities, additives, and heteroatomic contaminants that can poison or deactivate catalysts. These factors further complicate process stability and increase operational costs due to the need for frequent catalyst regeneration or replacement. These stringent conditions impose significant economic and practical limitations, particularly for large-scale implementation.

To overcome these limitations, nonthermal plasma (NTP)-assisted methods have been explored for plastic upcycling under significantly milder conditions.[11,14,29–32] NTP, particularly dielectric barrier discharge (DBD) plasma, offers a unique approach to breaking C–C bonds under ambient temperature and pressure conditions.[33] In NTP-assisted polymer hydrogenolysis, DBD-generated hydrogen plasma produces a mixture of energetic electrons, hydrogen atoms and radicals, excited hydrogen molecules, and hydrogen ions, with electrons possessing significantly higher energy than the surrounding gas molecules. These reactive plasma species effectively cleave polymer chains without requiring catalysts or solvents.[11,33] However, despite these advantages, one of the most persistent challenges of NTP-assisted hydrogenolysis is its historically low energy efficiency. Previous studies, including our own earlier work, have consistently reported output energy levels significantly lower than the electrical input energy. This discre-

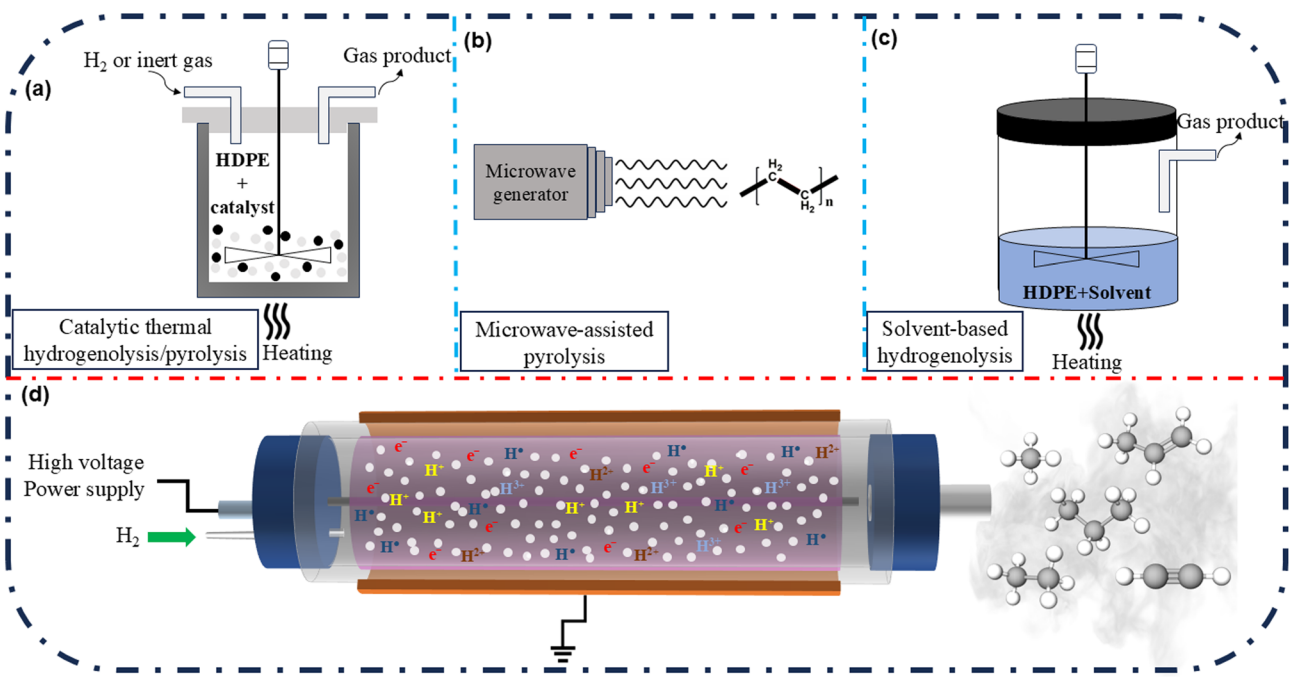

Fig. 1 (a–c) Overview of conventional methods for HDPE upcycling and (d) schematic illustration of the DBD reactor system used in this study for NTP-assisted HDPE hydrogenolysis.

pancy raises concerns about whether the process can achieve the energy efficiency and economic viability required for real-world applications.[11,14,31–33] For example, our previous study on NTP-assisted hydrogenolysis of PE demonstrated an energy consumption efficiency of less than 0.25 g kWh^{-1} at an input power of 60 W.[14] Similarly, El-Shafie *et al.* examined ammonia decomposition using DBD reactors and reported that the energy efficiency of a noncatalytic DBD reactor, defined as the ratio of output to input energy, was only 0.8.[34] Liu *et al.* also utilized a DBD reactor to decompose toluene, serving as a model compound for biomass tar. The noncatalytic reaction, conducted at an input power of 35 W, achieved an energy efficiency of less than 2 g kWh^{-1}.[35] This skepticism arises from the inherent nature of plasma systems, where generating the plasma species capable of breaking polymer bonds requires a high AC voltage, which can result in low electrical energy utilization efficiency. In conventional DBD systems, only a fraction of the supplied electrical energy is effectively converted into chemically reactive species, with substantial energy losses occurring through dielectric heating and non-productive plasma discharges. These inefficiencies have led many researchers to question whether NTP-assisted hydrogenolysis can overcome these fundamental barriers and achieve practical energy efficiency levels for large-scale plastic upcycling.

In this study, we present for the first time a highly energy-efficient and scalable DBD non-thermal plasma (NTP) reactor capable of rapid hydrogenolysis of both pure and real waste HDPE into light hydrocarbons (C_1–C_4) under ambient conditions (Fig. 1d). This achievement marks a significant advancement in NTP-assisted plastic upcycling technology. By integrating reactor and reaction engineering, we overcome the long-standing challenges of low polymer throughput and poor energy efficiency that have limited previous studies. These results demonstrate that NTP can serve as a viable and industrially scalable method for plastic conversion. Unlike prior work, our study systematically optimizes DBD reactor design and operational conditions to precisely control plasma generation, kinetics, spatial distribution, and plasma–polymer interactions. This approach ensures efficient energy utilization and enhanced reaction performance. We investigate key reactor configuration parameters (outer diameter, OD; plasma zone length, PZL) and operational parameters (HDPE loading density, input power, and reaction time) to develop a strategic framework for maximizing energy transfer and driving selective bond cleavage. Our optimized, scalable tubular reactor design, combined with fine-tuned reaction parameters, enables substantially higher HDPE loading and complete polymer conversion. This configuration achieves unprecedented energy efficiency, with a record output-to-input energy ratio of 8.2. This is the first study to conclusively demonstrate that NTP-assisted hydrogenolysis can achieve both high efficiency and scalability. These findings overturn skepticism about its economic feasibility and establish a transformative pathway for sustainable, energy-efficient plastic upcycling.

Experimental

Materials

HDPE powder (Sigma-Aldrich, USA) was used as the feedstock for NTP-assisted hydrogenolysis, while HDPE-based pill containers (Fig. S1) were examined as real waste HDPE samples. Quartz wool (Thermo Fisher Scientific, UK) was used to secure the HDPE pellet particles inside the DBD reactor, ensuring uniform exposure to plasma. High-purity hydrogen gas (99.999%) was supplied by Airgas. Following the hydrogenolysis reaction, 2,5-dihydroxybenzoic acid (Bruker, Germany) was used as the matrix, while 1,2,4-trichlorobenzene (≥99%, Sigma-Aldrich, China) and acetonitrile (99.9%, Sigma-Aldrich, USA) were used as solvents to prepare samples for matrix-assisted laser desorption/ionization-time of flight mass spectrometry (MALDI-TOF MS).

Nonthermal plasma-assisted hydrogenolysis of HDPE

NTP-assisted hydrogenolysis experiments were carried out using three quartz-tube DBD reactors with varying outer diameters (OD = 17, 42, and 50 mm), each powered by an AC power supply (30 kV) peak-to-peak voltage and frequency of 20 kHz to generate hydrogen plasma for HDPE hydrogenolysis. Plasma was generated within the plasma zone, defined by a copper tape ground electrode wrapped around the quartz tube and a tungsten rod as high-voltage electrode positioned inside the reactor (Fig. 1d). The plasma zone volume varied across experiments based on the reactor's inner diameter and plasma zone length. The maximum reaction temperature was 121 °C (Fig. S2) measured by an infrared thermal camera (Vevor).

To access reactor performance and reaction efficiency, 2 to 66 g of HDPE pellets (125–250 μm in size) were loaded into the DBD reactor, and experiments were conducted under a H_2 flow rate of 350 mL min^{-1} and a H_2 partial pressure of 101 kPa as standard conditions. To systematically investigate the effects of reaction time and input power, experiments were performed with reaction times ranging from 2.5 to 20 min and input power levels of 60, 70, and 80 W. Each experiment was repeated three times to ensure data reliability and statistical accuracy.

The mass of gas product was determined by measuring the weight loss of the reactor before and after the reaction, while the wax product was collected and weighed at the end of each experiment. The product distribution (Y, wt%) was calculated by the following equation:

$$Y = \frac{m_{\text{gas}}(\text{or } m_{\text{wax}})}{m_{\text{HDPE}}} \times 100\% \quad (1)$$

where m_{HDPE}, m_{gas}, and m_{wax} represent the mass of loaded HDPE, gas product, and wax product, respectively.

Product characterization and energy calculation

The outlet of the DBD tubular reactor, where HDPE hydrogenolysis occurs, was connected to an online mass spectrometer (Stanford Research Systems UGA-300) for real-time analysis

and quantification of gas products. The number of moles of saturated hydrocarbons produced during the reaction was used to evaluate hydrogen consumption, enabling the calculation of energy consumption due to hydrogen usage (eqn (S2)). This energy, combined with the electrical input energy (calculated as power × reaction time, eqn (S3)), constituted the total input energy. Since this study primarily focuses on gas product quantification, the output energy was determined by multiplying the mass of each gas product by its heat of combustion (Table S1), providing the total output energy based solely on gas-phase products (eqn (S4)). As the contribution of the wax product was not included in the output energy calculation, the reported values represent a slight underestimation of the total energy output.

The wax product was characterized by MALDI-TOF MS with a Bruker Ultraflex II MALDI-TOF/TOF instrument. For sample preparation, HDPE and wax products were dissolved in trichlorobenzene and 2,5-dihydroxybenzoic acid, used as the MALDI matrix, was dissolved in acetonitrile at concentrations of 1 mg mL^{-1} and 3 mg mL^{-1}, respectively. A 0.5 μL aliquot of the wax solution and 0.5 μL of the matrix solution were dropped onto the sample plate and air-dried at room temperature. Positive ion MALDI-TOF MS spectra of wax samples were recorded in reflectron detection mode, with an accelerating voltage of 20 kV, laser intensity of 60%, and 5000 total laser shots. The detection range was set from 0 to 6000 Da.

To identify high-energy plasma species and monitor reactor temperature during NTP-assisted hydrogenolysis of HDPE, optical emission spectroscopy (OES, Ocean Optics USB4000 with fiber optic cable) and an infrared thermal camera (Vevor) were employed, respectively.

Results and discussion

Product distribution and reaction pathway

Before evaluating the reactor's efficiency and energy output, it is essential to first determine the product distribution and the reaction pathways responsible for their formation. Understanding these aspects provides valuable insight into how reaction conditions influence product yields and overall performance. To establish baseline conversion behavior, experiments were conducted using the smallest reactor tube (OD = 17 mm), the shortest plasma zone length (PZL = 8 cm), and the lowest HDPE loading (2 g). As shown in Fig. 2a, the HDPE conversion reached 100% within 10 min of reaction, yielding 40.1% gas products and 59.9% wax products. The combination of low polymer loading and a shorter PZL enhanced polymer-to-gas conversion, increasing the proportion of gas-phase hydrocarbons.[14,31]

In situ gas analysis (Fig. S3) revealed that the gas product consisted of C_1–C_4 saturated hydrocarbons (CH_4, C_2H_6, C_3H_8, and C_4H_{10}) and unsaturated hydrocarbons (C_2H_2, C_2H_4, and C_3H_6). Notably, the gas composition was dominated by saturated hydrocarbons, particularly CH_4. The excessive formation of CH_4 remains a significant challenge in HDPE hydrogenolysis, as deep dehydrogenation and terminal C–C bond cleavage lead to high CH_4 yields, even when using conventional metal catalysts like Ru and Pt.[36–40] Addressing this issue requires catalyst design and process optimization to suppress overcracking and enhance the yield of heavier hydrocarbons.[36] MALDI analysis of HDPE and the wax products (Fig. 2a) confirms polymer chain cleavage, as indicated by the shift in the m/z distribution peak from 4560 for HDPE to 1880 for the wax product, further supporting the formation of both gas and wax products during NTP-assisted hydrogenolysis.

The optical emission spectrum (OES) collected during NTP-assisted hydrogenolysis of HDPE is shown in Fig. 2b. Prominent emission features include peaks at 609 nm and 656 nm, corresponding to excited molecular hydrogen (H_2) and atomic hydrogen (H_α, $n = 3 \rightarrow n = 2$ transition), respectively. The presence of H_α emission indicates effective electron impact dissociation of H_2 that generates reactive hydrogen radicals ($^{\bullet}H$), which can effectively drive the hydrogenolysis of HDPE.[41–44] The emission band observed at 430 nm is attributed to the $^{\bullet}CH$ radical ($A^2\Delta \rightarrow X^2\Pi$ transition), confirming active interactions between energetic electrons, hydrogen species, and hydrocarbon fragments derived from HDPE decomposition.[45] These $^{\bullet}CH$ radicals may originate from the fragmentation of small hydrocarbons (such as CH_4, C_2H_4, and C_2H_2), hydrogen abstraction from larger fragments, or recombination of C and H radicals within the plasma environment.[45,46] Additionally, the detection of C_2 Swan band ($D^3\Pi_g \rightarrow A^3\Pi_\mu$), particularly near 516 nm in the visible region, indicates further breakdown of HDPE and evolution of carbonaceous fragments into the gas phase. These bands arise from the formation of C_2 *via* recombination or secondary fragmentation of smaller carbon species (such as CH and C_2H_2), supporting the occurrence of deep molecular fragmentation during NTP-assisted hydrogenolysis.[44,46,47]

A plausible reaction pathway, based on both the experimental observations in this study and our previous work,[14] is illustrated in Fig. 2c. NTP-assisted HDPE hydrogenolysis likely initiates with the disruption of the polymer structure through bombardment by high-energy species generated in the hydrogen plasma, including electrons, protons, excited hydrogen molecules, and hydrogen radicals. These reactive species induce C–C bond cleavage at both end-chain and mid-chain positions. End-chain cleavage generates small hydrocarbon radicals ($^{\bullet}C_xH_y$) and short polymer fragments, while mid-chain cleavage predominantly produces wax-like oligomers, which can further degrade into smaller radicals under continued plasma exposure. These radicals likely follow two competing pathways: (1) hydrogenation, in which $^{\bullet}C_xH_y$ reacts with $^{\bullet}H$ to form saturated alkanes, and (2) recombination, where $^{\bullet}C_xH_y$ combine to produce longer-chain hydrocarbons. Under hydrogen-rich conditions, the process is thermodynamically driven toward hydrogenation, favoring the formation of saturated alkanes. Thermodynamic analysis (Table S2) supports this mechanism, showing that the Gibbs free energy ($\Delta G°$) for HDPE hydrogenolysis to alkanes is highly negative, indicating a spontaneous and energetically favorable process. In

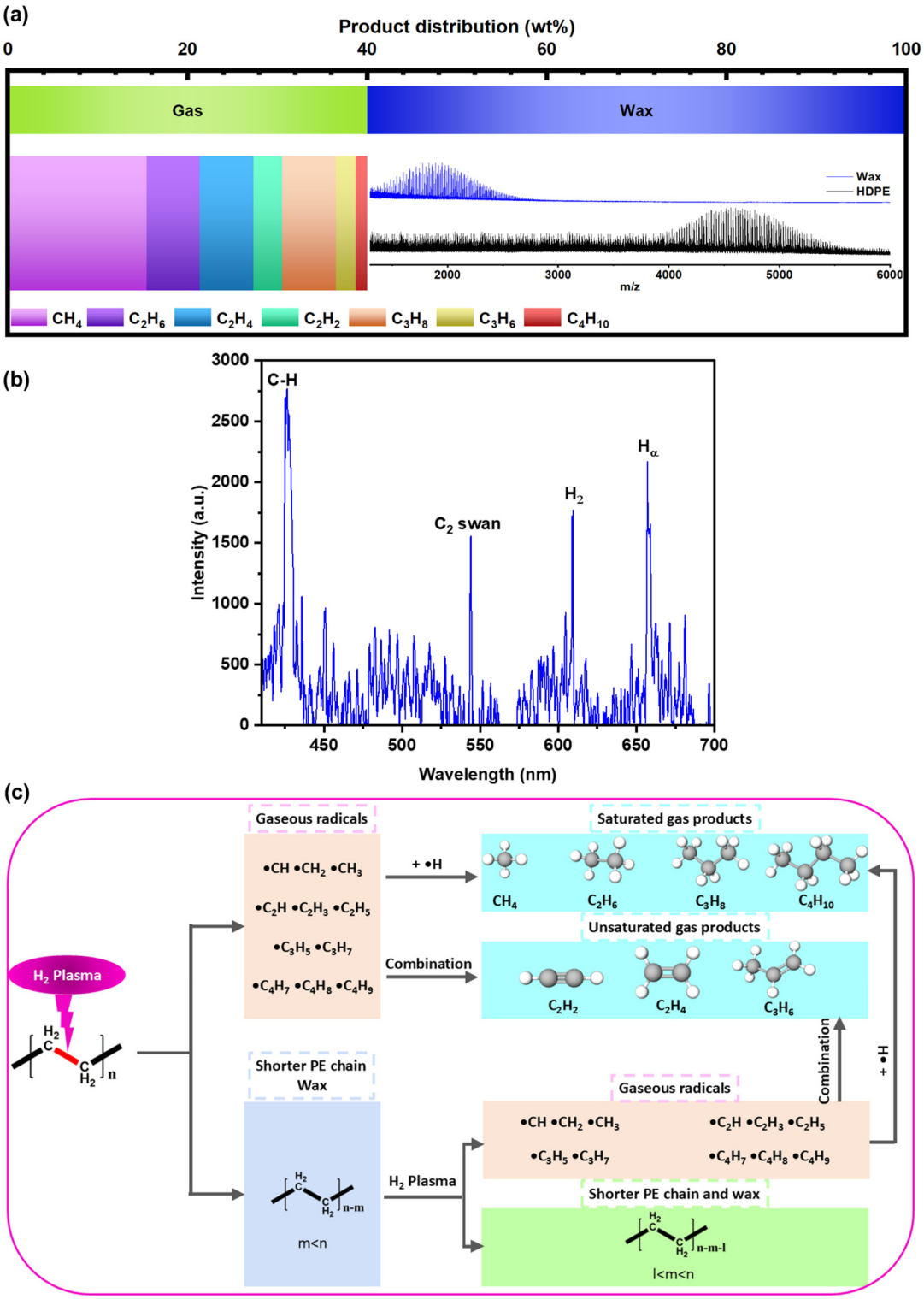

Fig. 2 (a) Gas and wax product yields from NTP-assisted HDPE hydrogenolysis, along with MALDI spectra of the initial HDPE and resulting wax product (reactor OD = 17 mm, PZL = 8 cm, HDPE loading density = 0.188 g cm^{-3}, input power = 60 W, reaction time = 10 min), (b) OES of the hydrogen plasma during HDPE hydrogenolysis showing key reactive species, and (c) proposed reaction pathways illustrating plasma-induced bond cleavage and product formation mechanisms.

contrast, the formation of unsaturated products exhibits less negative or slightly positive $\Delta G°$ values, making their production thermodynamically less favorable under the given conditions.

Effects of field strength and HDPE loading density on product distribution and energy efficiency

Results showed that increasing the reactor outer diameter (OD) from 17 mm to 50 mm, while maintaining a constant HDPE mass of 2 g, led to a decrease in gas product yield and output energy (calculated based on the total gaseous products). A slight reduction in input energy was also observed (Fig. 3a), mainly due to lower hydrogen consumption (Fig. S4). This suggests reduced interaction between the reactive species and polymer chains in the larger reactor. Consequently, the output-to-input energy ratio also decreased with increasing OD, remaining below 1 for all conditions at this low HDPE loading. These observations confirm the poor energy efficiency of NTP hydrogenolysis at low polymer loadings, consistent with previous studies.[11,14,31–33]

This observed decline in performance can be attributed to the effect of reactor OD on electric field strength and plasma species density. A larger OD increases the interelectrode distance, which in turn reduces the electric field strength and lowers the volumetric density of reactive plasma species.[48,49] Calculations showed that the electric field strength decreased from 31.2 kV cm^{-1} to 9.9 kV cm^{-1} as the OD increased from 17 mm to 50 mm (assuming the plasma zone is fully packed with HDPE pellets). This reduction led to the generation of less energetic and less dense plasma species, which further affected hydrogenolysis performance. First, the lower-energy plasma species reduced the turnover frequency (TOF) of hydrogenolysis, thereby lowering the reaction efficiency. Second, the decrease in plasma species density, coupled with the reduction in HDPE loading density from 0.188 g cm^{-3} to 0.015 g cm^{-3}, significantly reduced the collision probability between plasma

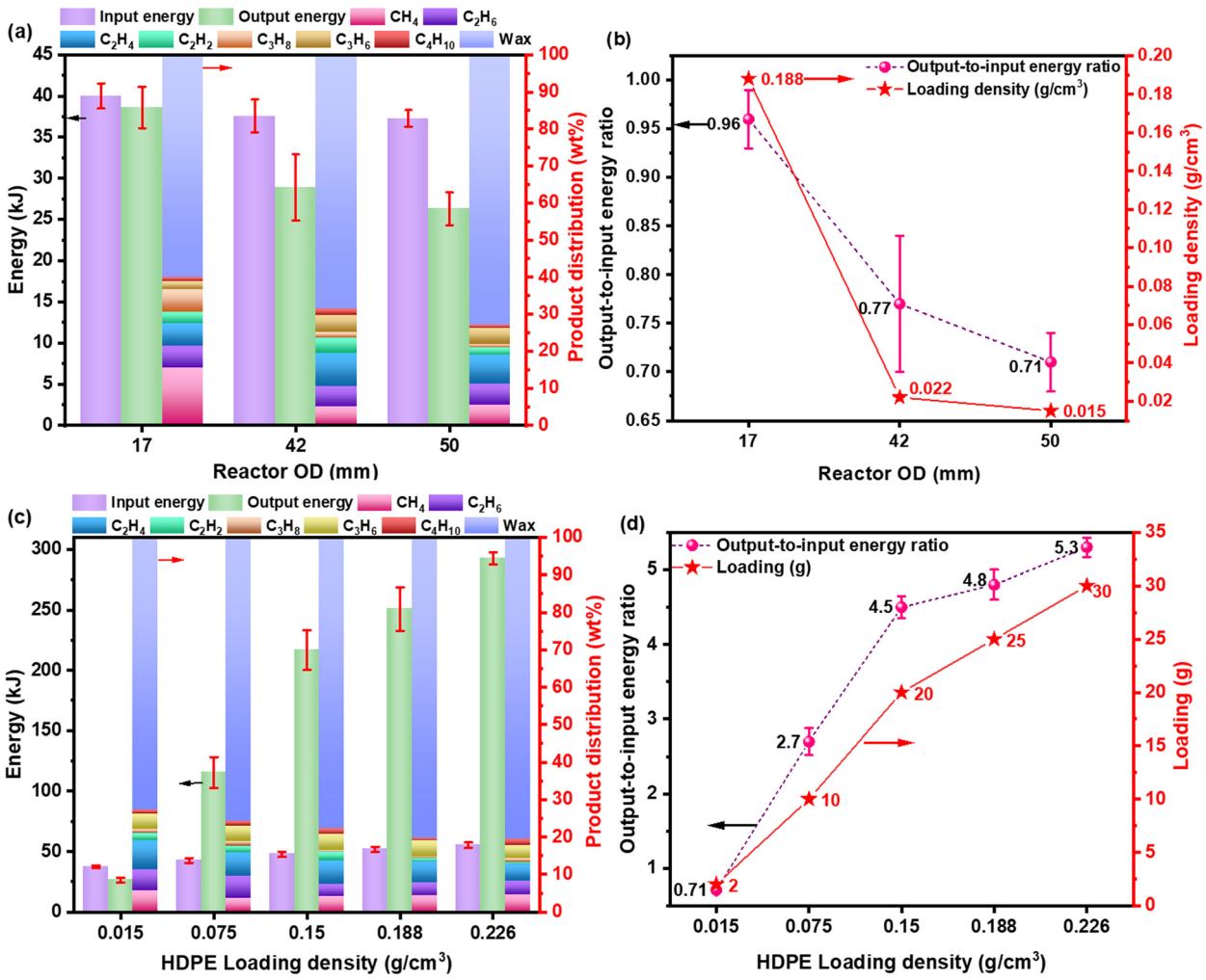

Fig. 3 Effects of DBD reactor OD on (a) input energy, output energy, and product distribution, and (b) output-to-input energy ratio during NTP-assisted hydrogenolysis of HDPE (PZL = 8 cm, HDPE loading = 2 g, input power = 60 W, reaction time = 10 min). Effects of HDPE loading density on (c) input energy, output energy, product distribution, and (d) output-to-input energy ratio (OD = 5 mm, PZL = 8 cm, input power = 60 W, reaction time = 10 min).

species and polymer molecules. The combined effect of these factors resulted in lower gas product yields and reduced hydrogenolysis efficiency as the reactor OD increased.

Interestingly, increasing the HDPE loading density in the 50 mm OD reactor, while keeping the PZL fixed at 8 cm, significantly improved the output energy and energy efficiency (Fig. 3c and d). As the HDPE loading increased from 2 g to 30 g, corresponding to a loading density increase from 0.015 g cm^{-3} to 0.226 g cm^{-3}, the total gas yield gradually declined from 27.1 wt% to 19.3 wt%. Although the gas yield percentage decreased, the absolute mass of gaseous products increased, resulting in higher input energy due to elevated H_2 consumption (Fig. S5). This indicates stronger interactions between energetic reactive species and HDPE chains within the reactor, leading to a significant increase in H_2 consumption and output energy. As a result, the output-to-input energy ratio increased to 5.3 for 0.226 g cm^{-3}, which is 7.5 times higher than that for 0.015 g cm^{-3}. This improvement in energy efficiency is attributed to packing effects. At low loading densities, plasma discharge is dominated by long filamentary discharges in the voids between HDPE pellets, resulting in inefficient plasma–polymer interactions. At higher loading densities, the denser packing shifts plasma discharges to surface and local filamentary modes, which are more effective at generating reactive species.[50,51] These surface and micro-discharges enhance the interaction probability between plasma species and polymer molecules, leading to better plasma utilization and overall energy efficiency. It should be noted that, as mentioned earlier, only gas products are considered to calculate the output energy; therefore, by including the energy of wax products, the output-to-input energy ratio could be even higher. Since the input energy remains unchanged, the inclusion of wax combustion energy would increase the numerator of the ratio, leading to a higher apparent energy efficiency.

The effect of electric field strength on energy efficiency was evident by comparing output-to-input energy ratios at a fixed HDPE loading density of 0.188 g cm^{-3}. As reactor OD increased from 17 mm to 50 mm, the ratio increased from 0.96 to 4.8, reflecting a trade-off between electric field strength and energy efficiency. On one hand, a stronger electric field generates more energetic plasma species, which enhances reaction kinetics and TOF. On the other hand, excessively energetic plasma species reduce energy utilization efficiency, as a significant portion of the input energy is dissipated instead of being effectively used for hydrogenolysis. Therefore, optimizing the electric field strength is essential to balance reaction efficiency and energy consumption, ensuring that sufficiently energetic plasma species are generated without incurring excessive energy waste.

Effects of plasma zone length, input power, and reaction time on product distribution and energy efficiency

After determining the optimal reactor OD, further optimization focused on identifying the ideal PZL, input power, and reaction time to maximize product yield and energy efficiency. To maintain a nearly constant loading density (~0.22 g cm^{-3}) and ensure dense packing for enhanced microdischarges, the HDPE loading was increased from 30 g to 66 g as the PZL was extended from 8 cm to 20 cm (Fig. 4a and b).

As shown in Fig. 4a, increasing the PZL from 8 cm to 16 cm led to a modest decline in total gas yield (from 19.3 wt% to 17.5 wt%), with a nearly constant alkane-to-alkene ratio and slightly lower methane production. However, when the PZL exceeded 16 cm, the gas yield dropped significantly, to 11.5 wt% at 18 cm and 9.1 wt% at 20 cm, alongside a noticeable increase in unsaturated hydrocarbons. Interestingly, despite the modest reduction in gas yield up to 16 cm, the output-to-input energy ratio improved significantly from 5.3 to 7.3, due to the greater gas mass produced from increased HDPE loading (Fig. 4b). This suggests that PZL plays a critical role in defining the plasma interaction volume and the residence time of hydrogen within the discharge zone, both of which are essential for enhancing plasma–polymer interactions, reaction kinetics, and energy utilization efficiency.[52,53] H_2 consumption data (Fig. S6) further support this trend, showing increased H_2 utilization with longer PZL up to 16 cm. The extended discharge region enhances the residence time and interaction probability between energetic species generated from hydrogen and the HDPE chains. However, at PZLs of 18 cm and 20 cm, both gas product yield and energy efficiency declined sharply, and at 20 cm, 7.3 wt% of HDPE remained unreacted after 10 min. This decline suggests the existence of an optimal PZL, which corresponds to an ideal balance of plasma species density and H_2 residence time. At low PZL, the discharge region is spatially constrained, resulting in a highly concentrated plasma. This can lead to undesirable plasma–plasma interactions, where energetic species are consumed through self-recombination or quenching reactions, rather than participating in productive plasma–polymer interactions, thereby reducing plasma utilization efficiency. In contrast, excessively long PZL leads to dilution of plasma species and less efficient species generation, as more energy is diverted toward sustaining ionization of hydrogen molecules rather than driving chemical transformations. Therefore, the results confirm that PZL of 16 cm, with a corresponding HDPE loading of 54 g, represents an optimum configuration, maximizing plasma–polymer interaction, reaction efficiency, and ultimately energy utilization efficiency for NTP-assisted hydrogenolysis.

Increasing the input power from 60 W to 80 W (Fig. 4c and d) resulted in notable increases in total gas yield (from 17.5 wt% to 22.1 wt%), input energy (from 64.7 kJ to 83.8 kJ), output energy (from 475.0 kJ to 579.6 kJ), and H_2 consumption (Fig. S7). This enhancement is attributed to the generation of more reactive hydrogen species at higher input powers, which promoted stronger interactions between H radicals and HDPE chains resulting in an increase in H_2 consumption (Fig. S7). However, the output-to-input energy ratio declined from 7.3 to 6.9, revealing a trade-off between reaction acceleration and energy efficiency. This trend can be attributed to the increased plasma species density at higher power levels. While the elec-

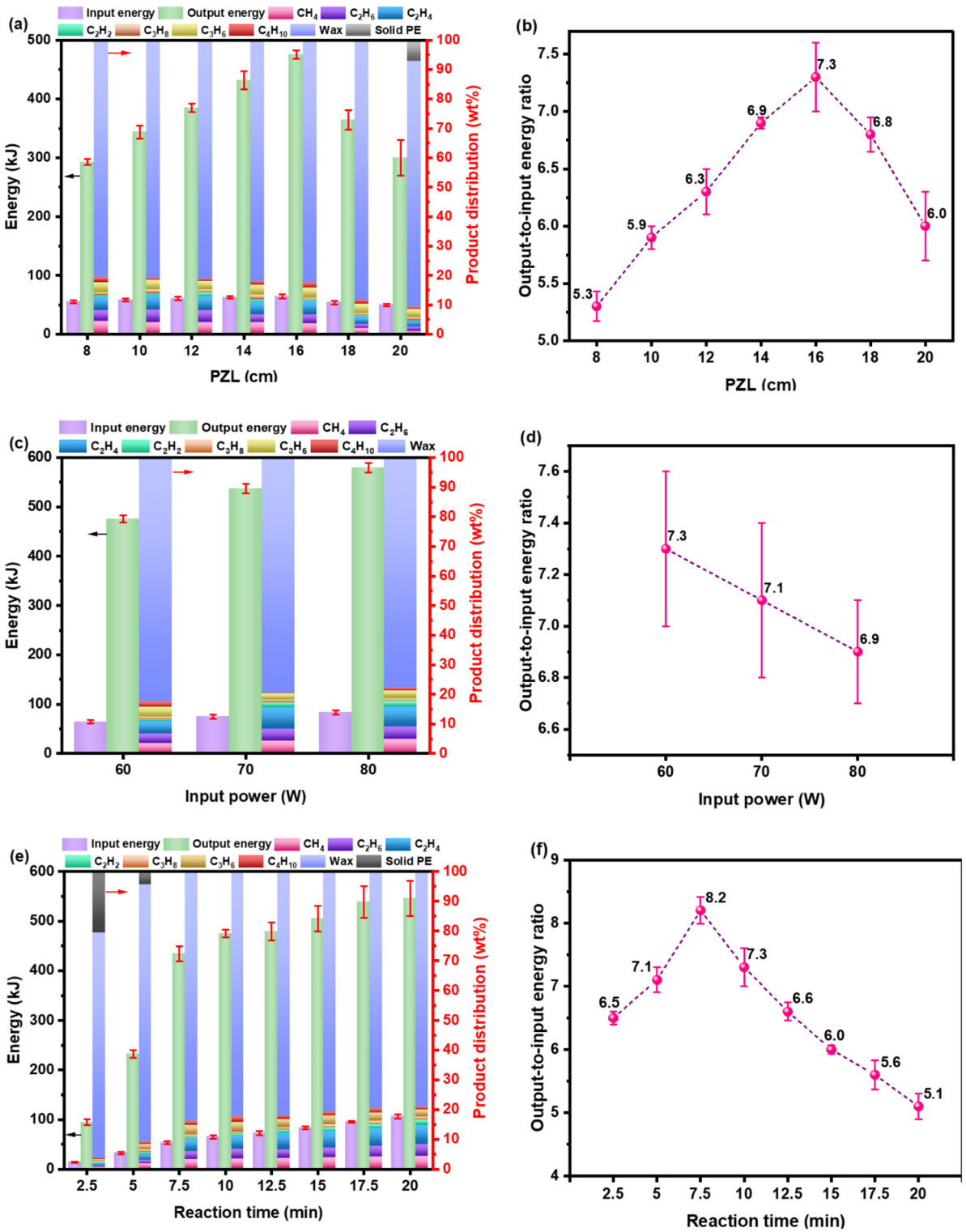

Fig. 4 Effects of key reaction parameters on input energy, output energy, product distribution, and output-to-input energy radio during NTP-assisted hydrogenolysis of HDPE: (a and b) PZL (OD = 50 mm, HDPE loading density = 0.22 g cm^{-3}, input power = 60 W, reaction time = 10 min), (c and d) input power (OD = 50 mm, PZL = 16 cm, HDPE loading density = 0.22 g cm^{-3}, reaction time = 10 min), and (e and f) reaction time (OD = 50 mm, PZL = 16 cm, HDPE loading density = 0.22 g cm^{-3}, input power = 60 W).

tric field strength remained largely unchanged, the higher power input generated a greater concentration of reactive species, including radicals and excited molecules, which enhanced the collision frequency and reaction rates within the plasma.[33,54] This facilitated more extensive C–C bond cleavage and hydrogenation reactions, especially the formation of satu-

rated alkanes, thereby increasing overall gas production and hydrogen consumption.[33] However, this enhancement came at a cost, *i.e.*, reduced energy utilization efficiency with the plasma species density exceeding the optimal range. At these high densities, plasma species increasingly interact with one another rather than with polymer molecules, resulting in non-productive recombination and quenching reactions, thereby dissipating energy without contributing to the hydrogenolysis process. This behavior mirrors the trends observed in the PZL experiments, where both insufficient and excessive plasma interaction volumes led to suboptimal energy efficiency due to imbalanced plasma species generation and utilization. Together, these findings emphasize the importance of identifying an optimal input power that maximizes plasma reactivity while avoiding overcrowding of reactive species, ensuring efficient energy use in NTP-assisted hydrogenolysis.

Similarly, increasing the reaction time from 2.5 min to 7.5 min led to a substantial increase in total gas yield (from 3.7 wt% to 16.1 wt%), as well as corresponding increases in output energy and the output-to-input energy ratio (Fig. 4e and f). HDPE conversion rose from 79.5% at 2.5 min to 95.8% at 5 min, and reached 100% at 7.5 min. At shorter reaction durations, the limited plasma exposure time was insufficient to cleave a significant number of C–C bonds, resulting in the formation of primarily wax-like products with higher molecular weights. This was confirmed by MALDI analysis, where the m/z peak of wax shifted from 2627 to 2051 as reaction time increased from 5 min to 10 min (Fig. S8), indicating progressive polymer breakdown. During the early stages of hydrogenolysis, gas-phase products were primarily generated through end-chain bond cleavage, which occurred less frequently than mid-chain scission. As a result, very short reaction times naturally yielded minimal gas.[11] Extending the reaction time to 7.5 min or longer ensured complete polymer conversion and substantially greater gas production. However, beyond 7.5 min, the output-to-input energy ratio began to decline, as the continued increase in energy input exceeded the incremental gains in output energy. This trend was mirrored in H_2 utilization which increased significantly with longer reaction times (Fig. S9). This occurred because the reactive species generated had more time and opportunity to participate in the reaction. Up to 7.5 min, the increased production of saturated hydrocarbons led to more efficient hydrogen consumption. Beyond this point, however, prolonged plasma exposure resulted in excess hydrogen being purged from the system without undergoing conversion, thereby reducing H_2 utilization efficiency. These findings indicate the existence of an optimal reaction time, beyond which the energetic cost outweighs the reaction benefits, reinforcing the need for careful time optimization to balance conversion, yield, and energy efficiency in NTP-assisted hydrogenolysis.

Hydrogenolysis of waste HDPE

The optimized conditions for NTP-assisted hydrogenolysis developed for maximizing energy efficiency with pure HDPE were applied to real waste HDPE sourced from pill bottles. As shown in Fig. 5, hydrogenolysis of the waste HDPE under identical reaction conditions resulted in 100% conversion and produced 20.6 wt% gaseous product, which is 3.1 wt% higher than that obtained for pure HDPE. The enhanced gas yield is likely due to structural differences in the waste HDPE. MALDI analysis (Fig. 5) revealed that the waste HDPE had a lower m/z peak (~3030) compared to the pure HDPE (~4560) used in this study, along with a broader molecular weight distribution (2400–4000 m/z). Following hydrogenolysis, the wax product derived from the waste HDPE exhibited shorter chain lengths than that from the pure HDPE, even under the same reactor conditions (Fig. 2). These shorter polymer chains contain a higher proportion of end-chain C–C bonds, which are more readily cleaved to promote higher gas production during the hydrogenolysis process.[18,55] Despite the increased gas yield, the overall gas composition remained similar, with saturated hydrocarbons as the dominant products, confirming the robustness and versatility of the DBD plasma system for the upcycling of real-world HDPE waste into valuable gaseous fuels. Waste HDPE commonly contains additives such as pigments and stabilizers, which can influence both thermal and plasma-assisted hydrogenolysis by modifying reaction environments or forming transient species and promoting secondary reactions. In this study, the HDPE waste contained stabilizers but no metal-based pigments. Despite the presence of stabil-

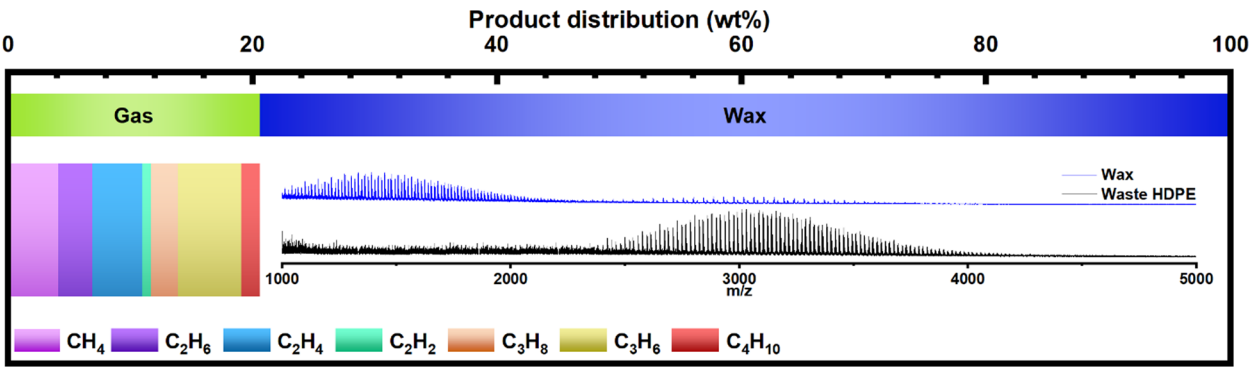

Fig. 5 Gas and wax product yields from NTP-assisted hydrogenolysis of waste HDPE, along with MALDI spectra of the initial waste HDPE and the resulting wax product (OD = 50 mm, PZL = 16 cm, HDPE loading density = 0.22 g cm^{-3}, input power = 60 W, reaction time = 10 min).

izers, the DBD reactor exhibited strong hydrogenolysis performance, suggesting good tolerance to minor impurities and reliable conversion efficiency under the tested conditions.

As shown in Fig. 6a, the slightly higher gas yield resulted from the hydrogenolysis of waste HDPE, compared to pure HDPE, translated into greater output energy. Although the

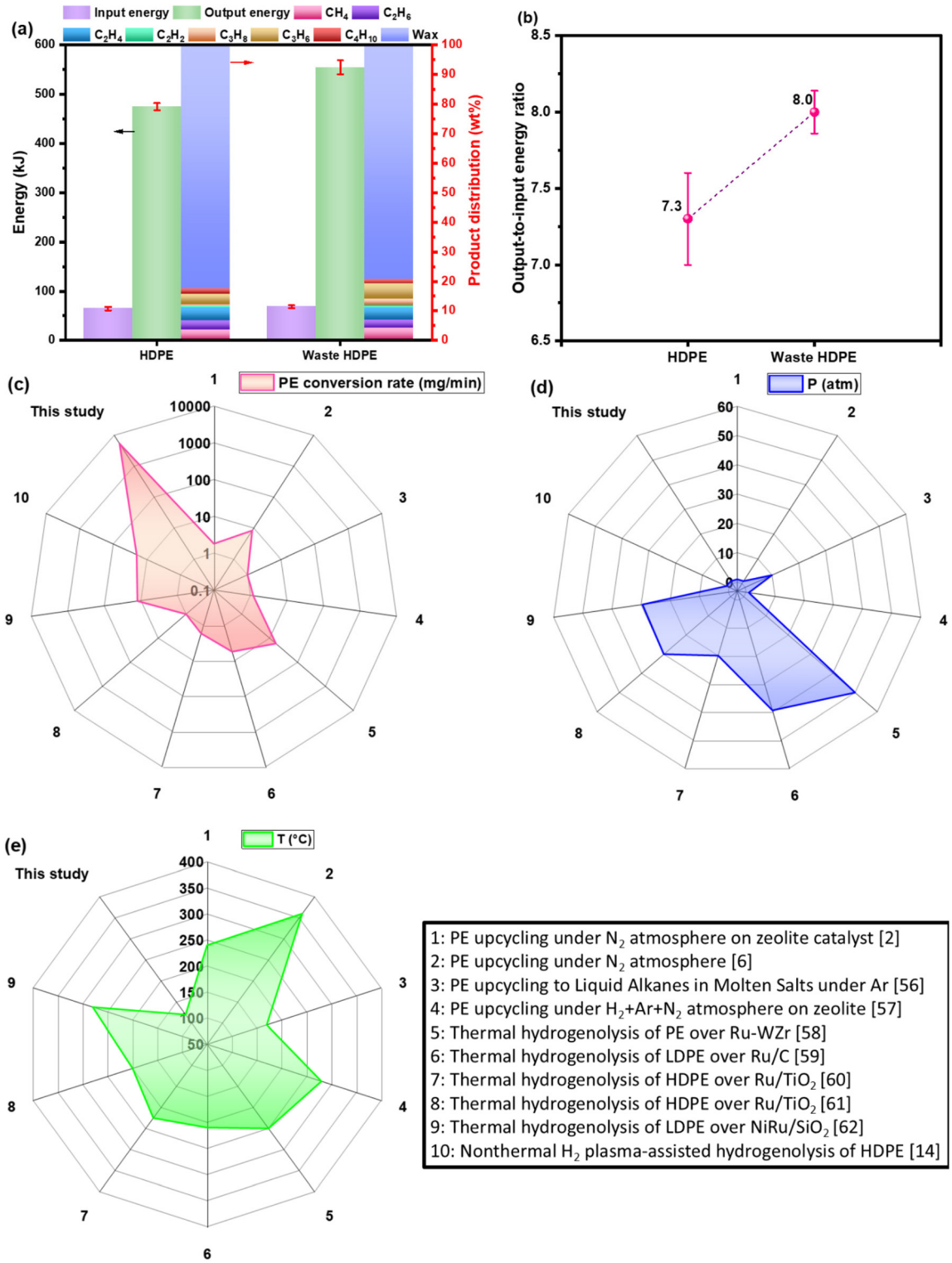

Fig. 6 (a) Input energy, output energy, and product distribution, and (b) output-to-input energy ratio for NTP-assisted hydrogenolysis of pure HDPE and waste HDPE using a DBD reactor (OD = 50 mm, PZL = 16 cm, HDPE loading density = 0.22 g cm^{-3}, input power = 60 W, reaction time = 10 min), (c) polyethylene conversion rate, (d) reaction pressure, and (e) reaction temperature achieved in this study compared with values reported in other methods from recent literature.[2,6,14,56–62]

input energy for waste HDPE hydrogenolysis was 4 kJ higher, primarily due to increased hydrogen consumption associated with the enhanced production of saturated hydrocarbons (Fig. S10), the larger gain in output energy led to an improved output-to-input energy ratio of 8.0 (Fig. 6b). Fig. 6c–e compare the HDPE conversion rate, reaction pressure, and operating temperature achieved in this work with recent literature reports employing both catalytic thermal methods and NTP techniques for polyethylene pyrolysis and hydrogenolysis.[2,6,14,56–62] As shown in Fig. 6c, our optimized DBD system reached a remarkably high conversion rate of 5400 mg min^{-1}, dramatically outperforming conventional thermal pyrolysis, catalytic hydrogenolysis, and even previously NTP-based studies, including our earlier work. Fig. 6d and e further illustrate the operational advantages of our approach. This high conversion rate was achieved under significantly lower hydrogen pressures and mild reaction temperatures, underscoring the unique benefits of NTP-assisted processing. While some recent studies have demonstrated PE depolymerization under atmospheric pressure using inert gases such as nitrogen,[2,6] they still required elevated temperatures (250–400 °C) and achieved limited conversion rates. In contrast, our system operates at ambient pressure and temperature, without the need for catalysts or external thermal input, enabling rapid, energy-efficient depolymerization under exceptionally mild conditions. Another important point concerning the literature on polyolefin hydrogenolysis is that most reported studies rely on the use of noble metal catalysts, such as Pt and Ru, to enhance the yield of gasoline- and diesel-range hydrocarbons having higher value compared to lighter hydrocarbons. However, these catalysts, particularly Ru, are also known to promote excessive methanation, leading to the formation of substantial amounts of methane.[56–62] This represents one of the major challenges in catalytic hydrogenolysis of polyolefins, as it decreases the carbon efficiency of the process. In contrast, our DBD plasma-assisted hydrogenolysis was conducted without any catalyst, which significantly limited methanation. Although the absence of a catalyst may result in lower yields of gasoline- and diesel-range hydrocarbons compared to catalytic systems, it eliminates the need for costly noble metals and reduces undesired methane formation. Furthermore, while quantification of the wax fraction was beyond the scope of this study, it is likely that a portion of these heavier hydrocarbons falls within the gasoline and diesel range, highlighting the potential of our noncatalytic plasma process for producing valuable fuel-range products from waste HDPE. Furthermore, the electricity cost for upcycling waste HDPE under the optimized condition was estimated to be as low as 2.7 ′ per kg, based on a power input of 60 W for 10 min, the average electricity rate of 14.41 ′ per kWh in South Carolina, USA, and the calculation in eqn (S4). These findings reinforce the potential of our scalable NTP platform as a low-energy and efficient solution for the upcycling of HDPE into valuable gaseous hydrocarbons.

Conclusions

In this study, we present the first demonstration of a highly energy-efficient, rapid, and scalable H_2 NTP system for the hydrogenolysis of HDPE. By integrating reaction engineering with mechanistic insights, we achieved complete polymer conversion under ambient conditions, yielding valuable C_1–C_4 gas products and wax, while significantly improving energy utilization efficiency.

Systematic optimization of reactor design and operating conditions, including reactor OD, PZL, HDPE loading density, input power, and reaction time, revealed critical mechanistic factors governing reactor performance. Increasing OD from 17 mm to 50 mm decreased electric field strength and plasma species density, reducing gas yields and output energy, which was calculated based solely on the combustion heat of the gaseous products. However, by increasing HDPE loading density to 0.226 g cm^{-3} at 50 mm OD, we enhanced plasma–polymer interaction probability, resulting in localized microdischarges that significantly boosted conversion efficiency and increased the output-to-input energy ratio to 5.3. Extending the PZL from 8 cm to 16 cm further raised this ratio to 7.3, driven by prolonged H_2 residence time and increased reactive species availability. However, beyond 16 cm, both gas yield and hydrogen utilization declined, as plasma species became overly diluted and the input electricity was increasingly spent on non-productive ionization. Increasing input power from 60 W to 80 W generated a higher density of reactive species, accelerating bond cleavage and increasing gas yield. However, this also led to plasma over-saturation, where radical recombination and plasma–plasma interactions became dominant, reducing energy utilization efficiency, evidenced by a drop in the energy ratio from 7.3 to 6.9. Similarly, reaction time played an important role, with short durations yielding low conversion and minimal gas due to insufficient plasma exposure to cleave mid-chain C–C bonds. 7.5 min was identified as the optimum duration, achieving 100% conversion and a peak output-to-input energy ratio of 8.2. Beyond this point, excess input energy outweighed gains in output energy, reducing efficiency. Mechanistically, these trends were supported by optical emission spectroscopy, which confirmed the formation of key reactive species, including H radicals, CH fragments, and C_2 species which are essential for polymer bond scission and gas formation. The reaction pathway, constructed from both current and previous studies, indicates that end-chain and mid-chain bond cleavage yields small hydrocarbon radicals, which undergo hydrogenation or recombination, with saturated alkanes favored under hydrogen-rich conditions.

The system's performance extended robustly to real HDPE waste, achieving 100% conversion, an even higher gas yield (20.6 wt%), and an energy efficiency ratio of 8.0. This enhanced performance is attributed to shorter chain lengths and higher end-chain bond content in the waste polymer, facilitating more efficient gas formation. When benchmarked against recent catalytic and NTP studies, our system achieved a record HDPE conversion rate of 5400 mg min^{-1} under ambient

pressure and temperature. The electricity cost for hydrogenolysis was estimated at just 2.7 cents per kg.

This technology holds strong potential for practical industrial applications, such as decentralized plastic waste upcycling and integration within circular carbon systems. Its ability to achieve efficient, catalyst-free hydrogenolysis under mild conditions highlights its promise as a sustainable and scalable approach for converting plastic waste into valuable hydrocarbons. To fully realize this potential, further efforts are needed to scale up the reactor design, ensure long-term process stability under continuous operation, and explore catalytic coupling strategies to enhance selectivity toward desired products.

Altogether, these findings establish our DBD-NTP platform as a mechanistically guided, low-energy, and scalable solution for the sustainable upcycling of HDPE waste.

Author contributions

Parsa Pishva: investigation, formal analysis, methodology, validation, writing – original draft. Jinyao Tang: investigation. Yanlin Zhu: writing – original draft. Jochen Lauterbach: supervision, writing – review & editing. Zhenmeng Peng: conceptualization, supervision, funding acquisition, writing – review & editing.

Conflicts of interest

There are no conflicts to declare.

Data availability

All data supporting the findings of this study are available within the article and its supplementary information (SI). Supplementary information is available. Supplementary information includes reaction temperature measured by an infrared thermal camera, mass spectrum of the gas product, the effect of DBD reactor OD, loading density, PZL, input power, and reaction time on the hydrogen utilization, effect of reaction time on MALDI spectra of wax products, hydrogen utilization of NTP hydrogenolysis of HDPE and HDPE waste, the heat of combustion of all gas products, and thermodynamic properties for all reactants and products. See DOI: https://doi.org/10.1039/d5gc04228c.

Acknowledgements

We acknowledge the financial support of this work by National Science Foundation (2132178).

References

1 F. Zhang, M. Zeng, R. D. Yappert, J. Sun, Y.-H. Lee, A. M. Lapointe, B. Peters, M. M. Abu-Omar and S. L. Scott, *Science*, 2020, **370**, 437–441.
2 Z. Cen, X. Han, L. Lin, S. Yang, W. Han, W. Wen, W. Yuan, M. Dong, Z. Ma, F. Li, Y. Ke, J. Dong, J. Zhang, S. Liu, J. Li, Q. Li, N. Wu, J. Xiang, H. Wu, L. Cai, Y. Hou, Y. Cheng, L. L. Daemen, A. J. Ramirez-Cuesta, P. Ferrer, D. C. Grinter, G. Held, Y. Liu and B. Han, *Nat. Chem.*, 2024, **16**, 871–880.
3 M. Macleod, H. Peter, H. Arp, M. B. Tekman and A. Jahnke, *Science*, 2021, **373**, 61–65.
4 M. Shaker, S. S. Hamdani, T. S. Muzata and M. Rabnawaz, *Sci. Rep.*, 2024, **14**, 14371.
5 Y. Wang, T. Biddle, C. Jiang, T. Luong, R. Chen, S. Brown, X. Jie and J. Hu, *Chem. Eng. J.*, 2023, **465**, 142918.
6 Z. Xu, N. E. Munyaneza, Q. Zhang, M. Sun, C. Posada, P. Venturo, N. A. Rorrer, J. Miscall, B. G. Sumpter and G. Liu, *Science*, 2023, **381**, 666–671.
7 F. Gorky, A. Nambo, T. J. Kessler, J. H. Mack and M. L. Carreon, *Ind. Eng. Chem. Res.*, 2023, **62**, 19571–19584.
8 S. Kwon, J. Kang, B. Lee, S. Hong, Y. Jeon, M. Bak and S. K. Im, *Energy Environ. Sci.*, 2023, **16**, 3074–3087.
9 C. Jehanno, J. W. Alty, M. Roosen, S. De Meester, A. P. Dove, E. Y. X. Chen, F. A. Leibfarth and H. Sardon, *Nature*, 2022, **603**, 803–814.
10 N. Singh and T. R. Walker, *npj Mater. Sustain.*, 2024, **2**, 39114578.
11 L. Yao, J. King, D. Wu, J. Ma, J. Li, R. Xie, S. S. C. Chuang, T. Miyoshi and Z. Peng, *Nat. Commun.*, 2022, **13**, 885.
12 X. H. Yue, F. S. Zhang, L. X. Wu, C. C. Zhang and P. Qian, *Chem. Eng. J.*, 2022, **435**, 134622.
13 T. Tan, W. Wang, K. Zhang, Z. Zhan, W. Deng, Q. Zhang and Y. Wang, *ChemSusChem*, 2022, **15**, e202200522.
14 L. Yao, J. King, D. Wu, S. S. C. Chuang and Z. Peng, *Catal. Commun.*, 2021, **150**, 106274.
15 X. Zhao, M. Korey, K. Li, K. Copenhaver, H. Tekinalp, S. Celik, K. Kalaitzidou, R. Ruan, A. J. Ragauskas and S. Ozcan, *Chem. Eng. J.*, 2022, **428**, 131928.
16 G. Yadav, A. Singh, A. Dutta, T. Uekert, J. S. DesVeaux, S. R. Nicholson, E. C. D. Tan, C. Mukarakate, J. A. Schaidle, C. J. Wrasman, A. C. Carpenter, R. M. Baldwin, Y. Román-Leshkov and G. T. Beckham, *Energy Environ. Sci.*, 2023, **16**, 3638–3653.
17 H. Jung, G. Shin, H. Kwak, L. T. Hao, J. Jegal, H. J. Kim, H. Jeon, J. Park and D. X. Oh, *Chemosphere*, 2023, **320**, 138089.
18 G. Celik, R. M. Kennedy, R. A. Hackler, M. Ferrandon, A. Tennakoon, S. Patnaik, A. M. Lapointe, S. C. Ammal, A. Heyden, F. A. Perras, M. Pruski, S. L. Scott, K. R. Poeppelmeier, A. D. Sadow and M. Delferro, *ACS Cent. Sci.*, 2019, **5**, 1795–1803.
19 H. Wang and S. C. E. Tsang, *Cell Rep. Phys. Sci.*, 2024, **5**, 102075.
20 D. Pan, F. Su, C. Liu and Z. Guo, *Adv. Compos. Hybrid Mater.*, 2020, **3**, 443–461.
21 H. H. Shah, M. Amin, A. Iqbal, I. Nadeem, M. Kalin, A. M. Soomar and A. M. Galal, *Front. Chem.*, 2023, **10**, 960894.
22 S. S. Alam and A. H. Khan, *Int. J. Environ. Sci. Technol.*, 2024, **21**, 5311–5330.

23 Q. Hu, S. Qian, Y. Wang, J. Zhao, M. Jiang, M. Sun, H. Huang, T. Gan, J. Ma, J. Zhang, Y. Cheng and Z. Niu, *Nat. Commun.*, 2024, **15**, 10573.
24 Y. Nakaji, M. Tamura, S. Miyaoka, S. Kumagai, M. Tanji, Y. Nakagawa, T. Yoshioka and K. Tomishige, *Appl. Catal., B*, 2021, **285**, 119805.
25 C. Sun, J. Wang, J. Wang, M. Shakouri, B. Shi, X. Liu, Y. Guo, Y. Hu, X. P. Wu and Y. Wang, *Appl. Catal., B*, 2024, **353**, 124046.
26 A. S. de Souza, P. G. Ferreira, I. S. de Jesus, R. P. R. F. de Oliveira, A. S. de Carvalho, D. O. Futuro and V. F. Ferreira, *Molecules*, 2025, **30**, 87.
27 K. L. Sánchez-Rivera and G. W. Huber, *ACS Cent. Sci.*, 2021, **7**, 17–19.
28 J. Wang, E. Minami and H. Kawamoto, *RSC Sustainability*, 2023, **1**, 1192–1199.
29 J. Song, J. Lv, Y. Pan, J. Wang, J. Wang, A. Cao, A. Wu, P. T. Williams and Q. Huang, *Chem. Eng. J.*, 2024, **490**, 151676.
30 I. Aminu, M. A. Nahil and P. T. Williams, *Energy Fuels*, 2022, **36**, 3788–3801.
31 H. M. Nguyen and M. L. Carreon, *ACS Sustainable Chem. Eng.*, 2022, **10**, 9480–9491.
32 B. Tabu, K. Akers, P. Yu, M. Baghirzade, E. Brack, C. Drew, J. H. Mack, H. W. Wong and J. P. Trelles, *Int. J. Hydrogen Energy*, 2022, **47**, 39743–39757.
33 P. Pishva, J. Li, R. Xie, J. Tang, P. Nandy, T. Farouk, J. Guo and Z. Peng, *Chem. Eng. J.*, 2024, **501**, 157776.
34 M. El-Shafie, S. Kambara and Y. Hayakawa, *Int. J. Hydrogen Energy*, 2021, **46**, 29361–29375.
35 S. Y. Liu, D. H. Mei, M. A. Nahil, S. Gadkari, S. Gu, P. T. Williams and X. Tu, *Fuel Process. Technol.*, 2017, **166**, 269–275.
36 A. Musa, E. A. Jaseer, S. Barman and N. Garcia, *Energy Fuels*, 2024, **38**, 1676–1691.
37 L. Chen, L. C. Meyer, L. Kovarik, D. Meira, X. I. Pereira-Hernandez, H. Shi, K. Khivantsev, O. Y. Gutiérrez and J. Szanyi, *ACS Catal.*, 2022, **12**, 4618–4627.
38 M. Tamura, S. Miyaoka, Y. Nakaji, M. Tanji, S. Kumagai, Y. Nakagawa, T. Yoshioka and K. Tomishige, *Appl. Catal., B*, 2022, **318**, 121870.
39 X. Wu, A. Tennakoon, R. Yappert, M. Esveld, M. S. Ferrandon, R. A. Hackler, A. M. Lapointe, A. Heyden, M. Delferro, B. Peters, A. D. Sadow and W. Huang, *J. Am. Chem. Soc.*, 2022, **144**, 5323–5334.
40 S. Liu, P. A. Kots, B. C. Vance, A. Danielson and D. G. Vlachos, *Sci. Adv.*, 2021, **7**, eabf8283.
41 J. de Oliveira Mallia, S. Griffin, C. Buttigieg and R. Gatt, *Front. Chem.*, 2024, **12**, 1416982.
42 M. Imam, C. Höglund, S. Schmidt, R. Hall-Wilton, J. Birch and H. Pedersen, *J. Chem. Phys.*, 2018, **148**, 034701.
43 M. Y. Naz, S. Shukrullah, S. U. Rehman, Y. Khan, A. A. Al-Arainy and R. Meer, *Sci. Rep.*, 2021, **11**, 2896.
44 R. Z. Walker, S. Gershman, D. E. Doughty and J. E. Foster, *Plasma Processes Polym.*, 2024, **21**, 2300155.
45 H.-C. Hsueh, H.-C. Li, D. Chiang and S. Lee, *J. Electrochem. Soc.*, 2011, **159**, D77–D83.
46 P. Fazekas, A. M. Keszler, E. Bódis, E. Drotár, S. Klébert, Z. Károly and J. Szépvölgyi, *Open Chem.*, 2015, **13**, 549–556.
47 S. Zhang, X. Zeng, H. Bai, C. Zhang and T. Shao, *Spectrochim. Acta, Part A*, 2022, **267**, 120590.
48 J. Anuntagool, N. Srangsomjit, P. Thaweewong and G. Alvarez, *Food Control*, 2023, **153**, 109913.
49 S. Elaissi and K. Charrada, *Coatings*, 2021, **11**, 1405.
50 W. Wang, H. H. Kim, K. Van Laer and A. Bogaerts, *Chem. Eng. J.*, 2018, **334**, 2467–2479.
51 X. Li, L. Zhang, A. Shahzad, P. Attri and Q. Zhang, *Plasma*, 2023, **6**, 637–648.
52 M. Bahri, F. Haghighat, S. Rohani and H. Kazemian, *Chem. Eng. J.*, 2016, **302**, 204–212.
53 Y. Cai, L. Lu and P. Li, *Appl. Sci.*, 2020, **10**, 1–16.
54 Q. Lu, W. Lei, W. Yue, W. Huang, Y. Dong, W. Yan, Y. Liu, Y. Chen and Y. Zhao, *Fuel*, 2023, **344**, 128041.
55 R. Lemmens, J. Vercammen, L. Van Belleghem and D. De Vos, *Nat. Commun.*, 2024, **15**, 9188.
56 L. Qiu, F. Polo-Garzon, L. L. Daemen, M. J. Kim, J. Guo, B. G. Sumpter, M. R. Koehler, C. A. Steren, T. Wang, L. T. Kearney, T. Saito, Z. Yang and S. Dai, *J. Am. Chem. Soc.*, 2025, **147**, 16207–16216.
57 J. Duan, W. Chen, C. Wang, L. Wang, Z. Liu, X. Yi, W. Fang, H. Wang, H. Wei, S. Xu, Y. Yang, Q. Yang, Z. Bao, Z. Zhang, Q. Ren, H. Zhou, X. Qin, A. Zheng and F. S. Xiao, *J. Am. Chem. Soc.*, 2022, **144**, 14269–14277.
58 C. Wang, T. Xie, P. A. Kots, B. C. Vance, K. Yu, P. Kumar, J. Fu, S. Liu, G. Tsilomelekis, E. A. Stach, W. Zheng and D. G. Vlachos, *JACS Au*, 2021, **1**, 1422–1434.
59 W. Ma, C. Wang, Z. Chen, S. Yan, S. Cao, X. Wang, Y. Chen, H. Yang and H. Chen, *J. Energy Inst.*, 2024, **115**, 101615.
60 S. D. Jaydev, A. J. Martín, M. E. Usteri, K. Chikri, H. Eliasson, R. Erni and J. Pérez-Ramírez, *Angew. Chem., Int. Ed.*, 2024, **63**, e202317526.
61 T. Kim, H. Nguyen-Phu, T. Kwon, K. H. Kang and I. Ro, *Environ. Pollut.*, 2023, **331**, 121876.
62 X. Zhang, B. Sun, Z. Zhao, T. Li, M. Mate and K. Wang, *Front. Chem. Sci. Eng.*, 2024, **18**, 110.